

# Computational Estimation of the Yarkovsky Effect on Asteroid 101955 Bennu

John P. Basart<sup>1</sup>, Erik Goetzke<sup>2</sup>, Dalton Groath<sup>3</sup>, and Bong Wie<sup>4</sup>  
*Asteroid Deflection Research Center, Iowa State University, Ames, IA 50011, USA*

Version: August 20, 2014

It is thought that many asteroids in orbits close to the Earth have been moved from outer orbits by the Yarkovsky effect. The orbital change is caused by solar heat absorption and surface re-radiation, creating a recoil force on the asteroid that either increases or decreases the tangential orbital velocity depending upon prograde or retrograde asteroid rotation, respectively. Developing the mathematics to analytically calculate this radiated force is sufficiently complicated that it cannot be done without a number of approximations. Hence, we have taken a numerical approach to obtain more reliable solutions and evaluate the accuracy of published analytic solutions. Our approach uses the multiphysics software COMSOL, incorporating its heat transfer package and surface-to-surface radiation module to model the Yarkovsky effect on a spherical asteroid model with homogeneous material composition. For the asteroid Bennu the magnitude of the Yarkovsky force is estimated to be 0.083 N at an orbital distance of 0.897 AU (perihelion).

## 1. INTRODUCTION

There are hundreds of known asteroids whose orbits cross the Earth's orbit. One of these, asteroid 101955 Bennu with provisional designation 1999 RQ<sub>36</sub> (Bennu henceforth) has become an object of interest because of its possible collision with Earth in the latter part of the 22<sup>nd</sup> century[1]. With an aphelion distance of 1.356 AU (astronomical units) and perihelion distance of 0.897 AU, Bennu is sufficiently close for a spacecraft mission before the date of possible collision, for which NASA is planning for retrieving material samples from its surface in 2016. The orbits of Bennu and the Earth for January 1, 2015 are shown in Figure 1. Many gravitational perturbations are

---

<sup>1</sup>Professor Emeritus, Dept. of Electrical and Computer Engineering, 335 Durham Center.

<sup>2</sup>Research Assistant, Dept. of Aerospace Engineering.

<sup>3</sup>Research Assistant, Dept. of Aerospace Engineering.

<sup>4</sup>Vance Coffman Endowed Chair Professor, Dept. of Aerospace Engineering, 2355 Howe Hall.

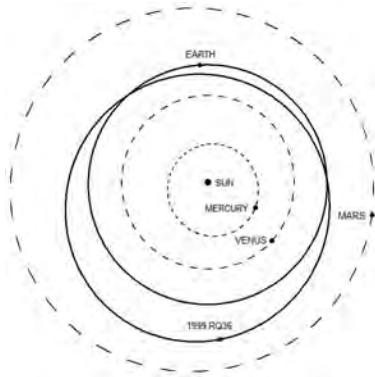


**FIG. 1** Orbits of Earth and RQ36 on Jan. 1, 2015.

considered when predicting a change in an asteroid’s orbit, but one nongravitational effect believed to be of significance is the Yarkovsky effect. This effect is a radiative force most prominent on small orbiting bodies. It is not effective on large bodies because the surface radiation increases as radius squared and the volume increases as radius cubed. Hence, the mass to accelerate increases faster than the radiation force. We reported our first numerical results of the Yarkovsky effect in 2012 [2]. Our recent work builds upon our previous work, but now we use a surface-to-surface radiation model whereas before we used a surface-to-ambient model. We report the change in Bennu’s orbit resulting from our temperature calculations.

A considerable amount of effort has been made, especially by Vokrouhlický, in finding analytic solutions [3]–[6] to this effect and how it influences an asteroid’s orbit. Due to the inherent nonlinearity in modeling the asteroid’s temperature rise from solar radiation, the theories become complex and require various assumptions for simplified solutions. More recently, however, there has been increased activity in using numerical methods to solve this problem as exemplified by Sekiya et al.[7], Rozitis and Green [8][9] and by Čapek and Vokrouhlický[10]. In [7], [8] and [9] there is still considerable analytic development before introducing numerical solutions to determine the temperature distribution and acting forces on the asteroid. However, in [10] heat equations are coded with a geometric model of an asteroid to determine an asteroid orbit change. The disadvantage of taking, or including, an analytic route in solving the Yarkovsky effect is that as the geometry becomes more complex, the solution will be more complex also; perhaps to the point where it becomes nearly impossible to solve analytically. Analytical solutions are important and useful for showing how the temperature fully depends upon the variables involved, but fully

numerical solutions can offer more elegant results, without introducing simplifications. The work we present in this paper for determining the asteroid temperature distribution is completely numerical. Instead of coding the problem ourselves, we have used the multiphysics software package COMSOL [11] in implementing this as part of our solution to the Yarkovsky effect.

While solving for the temperature of a rotating asteroid, we are also testing COMSOL to check its suitability for solving the asteroid heating problem. For the results presented in this paper, our model assumes the sphere to have homogenous material properties.

There is an growing amount of literature on Bennu due to the planned visitation. Some of the papers with extensive discussions of Bennu’s physical parameters and the Yarkovsky effect are [12]–[16]. The paper by Chesley et al. [16] especially has a rigorous discussion of determining the density of Bennu by combining radar observations with infrared observations. The values of thermal conductivity, specific heat, and density used in our temperature and force calculations come from Chesley et al. [16].

## 2. HEAT TRANSFER THEORY

We follow the approach given by Vokrouhlický [17] for formulating our governing equations. We assume emission arriving from the sun is a plane wave as if emitted from a point source. When it reaches the asteroid two things happen: 1) some energy is reflected, represented by the Bond albedo ( $1 - \alpha$ ), and 2) the remaining energy is absorbed (represented by an absorption coefficient,  $\alpha$ ). The absorbed energy heats the asteroid. The heat then flows two ways: 1) it conducts into the asteroid, and 2) the remaining heat radiates in the infrared portion of the spectrum via black-body radiation modified by an emission coefficient,  $\epsilon$ . Of interest to us is this radiated heat. The infrared rays, being electromagnetic waves, carry energy and momentum. The radiated momentum causes a recoil force on the asteroid. If it radiated in a direction only back towards the sun (the direction from which the solar rays came) there would be very little asteroid orbit change over a year. However, because of thermal inertia, the warmest part of the asteroid “day” is early “afternoon” as it is on the Earth if we neglect atmospheric effects. The radiation vector now has an additional component tangential to the orbit instead of only a normal component. This causes a force parallel or antiparallel to the orbit, the so-called Yarkovsky effect. (There is no reference to Yarkovsky himself since his discovery was documented only in notes.) The tangential component of radiation can either increase or decrease the size of the orbit. If

the asteroid rotation is in a prograde motion with respect to the orbit, the recoil force nudges the asteroid into a higher orbit, and conversely for retrograde motion.

The two commonly used equations for determining the temperature are the heat transfer equation

$$\rho C \frac{\partial T}{\partial t} = \nabla \cdot (k \nabla T) \quad (1)$$

and the boundary condition

$$\epsilon \sigma T^4 + k (\hat{\mathbf{n}} \cdot \nabla T) = \alpha \Phi \quad \text{at the surface} \quad (2)$$

where  $T$  is the temperature in Kelvins,  $\rho$  is the density,  $C$  is the specific heat,  $k$  is the thermal conductivity,  $t$  is the time,  $\sigma$  is the Stefan-Boltzmann constant,  $\Phi$  is the power density from the sun at the distance of the asteroid,  $\nabla$  is the gradient, and  $\hat{\mathbf{n}}$  is a unit vector normal to the surface. All units are in the SI system. In Equation (2) the temperature is to be evaluated at the boundary. If we assume heat transfer only in the radial direction, Eqs. (1) and (2) become

$$\rho C \frac{\partial T}{\partial t} = k \frac{\partial^2 T}{\partial r^2} \quad (3)$$

and

$$\epsilon \sigma T^4 + k \frac{\partial T}{\partial r} = \alpha \Phi \quad \text{at the surface} \quad (4)$$

respectively. Many journal papers dealing with the Yarkovsky effect are solving for temperature starting with these equations. The excessive difficulty solving for temperature lies with  $T^4$  in Equation (2). Our solution is strictly numerical with no further manipulations of the two equations. In our numerical work with COMSOL we permit surface-to-surface radiation. That is, if we have a crater on the surface of the model, one side of the crater may radiate towards another side of the crater. The boundary condition in COMSOL is then

$$-\hat{\mathbf{n}} \cdot (-k \nabla T) = \epsilon (G - \sigma T^4) \quad (5)$$

where

$$G = G_m(J) + F_{amb}\sigma T_{amb}^4 + F_{solar} |\mathbf{Q}| \quad (6)$$

and  $G$  is the total arriving radiative flux (in  $\text{W}/\text{m}^2$ ), a function of the radiation coming from other cell surfaces  $G_m(J)$ .  $F_{amb}$  is the ambient view factor,  $T_{amb}$  is the ambient temperature, and  $\mathbf{Q}$  is the external radiation source (the sun in this case). The external radiation source is a function of time allowing the model to rotate as shown in the following expression:

$$\mathbf{Q} = \alpha \frac{Q_0}{|\mathbf{r}|^2} \begin{bmatrix} -\cos(i) \cos(\frac{2\pi}{P}t) \\ \cos(i) \sin(\frac{2\pi}{P}t) \\ -\sin(i) \end{bmatrix} \quad (7)$$

where  $Q_0$  is the solar heat flux at 1 AU ( $1378 \text{ W}/\text{m}^2$ ),  $\mathbf{r}$  is the orbit position vector,  $P$  is the period of rotation of the asteroid, and  $i$  is the obliquity angle measured from  $\hat{\mathbf{W}}$  (unit vector normal to the orbital plane) to the spin axis and calculated by

$$i = \cos^{-1} \left( \frac{\mathbf{r} \cdot \mathbf{s}}{|\mathbf{r}| |\mathbf{s}|} \right) - \frac{\pi}{2}. \quad (8)$$

where  $\mathbf{s}$  is the spin axis vector in the same coordinate system as  $\mathbf{r}$  (PQW or ijk typically).

In the present paper we restrict our attention to homogeneous spheres so we reduce Equation (6) to

$$G = \sigma T_{amb}^4 + |\mathbf{Q}| \quad (9)$$

where  $G_m(J) = 0$ ,  $F_{amb} = 1$  and  $T_{amb} = 3 \text{ K}$ , the microwave background temperature, for lack of a better number. Consequently, Equation (5) becomes

$$\hat{\mathbf{n}} \cdot (k\nabla T) + \epsilon\sigma(T^4 - T_{amb}^4) = \epsilon |\mathbf{Q}|. \quad (10)$$

Equations (3) and (10) are used by COMSOL in solving for temperatures used in this paper.

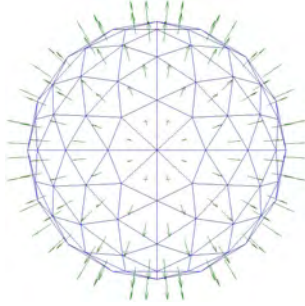


**FIG. 2** Vectors emanating normal to mesh segments. When written in terms of pressure they are vectorally summed to give the final force.

### 3. COMSOL

The approach we’ve taken to determine the surface temperature distribution needed to calculate the Yarkovsky Effect is fully dependent upon the COMSOL Multiphysics software with the heat transfer package. The software is well organized to help the user step through the process of setting up a model. The steps are: 1) select space dimension, 2) add physics module(s), 3) select study type, 4) build geometry, 5) select materials, 6) define boundary conditions, 7) build mesh, and 8) execute program.

Our model incorporates a three dimensional sphere using the physics of “heat transfer in solid bodies” and “surface-to-surface radiation” to simulate an asteroid in space. A “boundary heat source” is also required to mimic the plane-wave solar radiation. We set the maximum value to  $1378 \text{ W/m}^2$  (our results examine circular orbits at 1 AU) and taper it with a cosine distribution to the limb of the sphere. A time-dependent study is added to allow for the sphere to rotate while exposed to the heat source, in which we found 30 periods of rotation for each “run” to be sufficient in most cases.

Due to the limitations of finite element analysis, the geometry cannot rotate when exposed to the tapered heat source, but, considering relative motion, we let the boundary heat source move about the sphere in our model. Coordinate corrections are made in post processing of the surface temperature results to make it appear as if the sphere were rotating.

The type and strength of the meshing is important in achieving viable results. We use a free tetrahedral meshing (see Figure 2 for an example of meshing with a small amount of elements) in most cases, but a free triangular swept meshing was needed for a few of the larger bodies, as will be described in the results section later. The material properties we used, the same as Delbo

TABLE 1  
Material Properties

Property	Symbol	Value
Thermal conductivity	$k$	0.3 W/(m K)
Density	$\rho$	2000 kg/m <sup>3</sup>
Specific Heat at Constant Pressure	$C$	600 J/K
Optical Absorption Coefficient	$\alpha$	0.99
IR Emission Coefficient	$\epsilon$	0.9

and Michel [18], are listed in Table 1. Although recent papers by Nolan et al. [14], Emery et al., and [15] Chesley et al. [16] contain updated parameters, we followed through with our original parameters due to the vast amount of COMSOL runs that would have to be re-run to update our results.

One of the most important steps in building the asteroid model was to properly incorporate the boundary conditions and more specifically the moving heat source. Being that Bennu is sufficiently far from the sun, a uniform plane wave of incoming radiation was assumed. To simulate this plane wave on the surface of the sphere, a cosine distribution was used on the model to taper the illumination from the subsolar point to the poles and limbs of the sphere. Keeping the asteroid at a distance of 1 AU from the sun, the maximum heat flux was 1378 W/m<sup>2</sup>. As mentioned before with limits on finite element analysis, the geometry and meshing cannot move, but the boundary conditions were manipulated to do so. This was done using coordinate transformations during COMSOL's iterations and then correcting this to appear as if the asteroid were rotating by counter coordinate transformations in post processing of the temperature data.

The last thing required to simulate the temperature development of an asteroid was an initial temperature of the starting body, which, when appropriately defined, drastically cut down the number of periods of rotation required to reach equilibrium values. Most of these steps have substeps incorporated.

#### 4. EXAMPLE FOR HOMOGENEOUS SPHERE

Figure 3 shows an example of the final temperature distribution calculated on a sphere by COMSOL. The hottest region is white and the coolest regions are red. In this case, the diameter is 2 meters and is 2 m in all following graphs unless stated otherwise. The period of rotation is 72,000 seconds, the spin axis is at an obliquity of 90<sup>0</sup>, and the orbital position vector is along

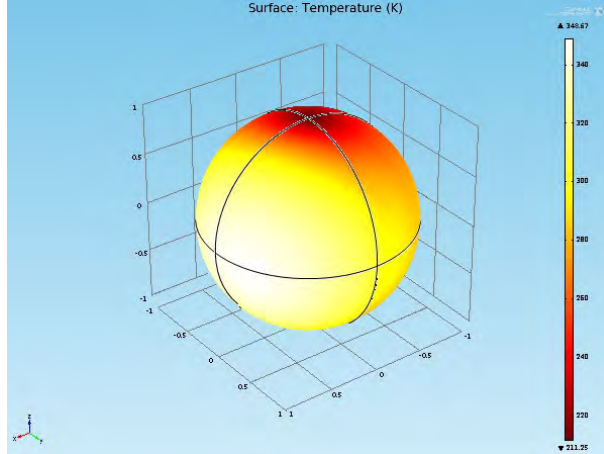


**FIG. 3** Temperature distribution over CCW rotating homogeneous sphere with hotspot to the right of subsolar point (coordinate intersection on left).

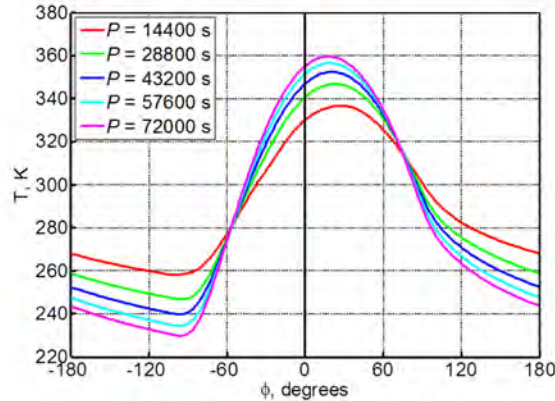


**FIG. 4** Equatorial surface temperature for various periods of rotation. Phi = 0 is the subsolar point.

the x-axis with a magnitude of 1 AU. (A small sphere with 2-m radius was chosen for many of the calculations because of the long computation time for a sphere the size of Bennu. When larger spheres are used it is specifically notated.) A more quantitative display of the temperature change is shown in Figure 4, a plot of the surface temperature distribution along the equator (coincident with the x-y plane for  $90^\circ$  obliquity) for this case and several periods of rotation. The 0 degree mark coincides with the sub-solar location. The hottest location in each of the cases is clearly offset by some angle from this point in the 15-30 degree range. As the period of rotation increases, the peak of the curve shifts to the left (nearer to the subsolar point) as expected. The peak temperature increases and the trough temperature decreases as the period

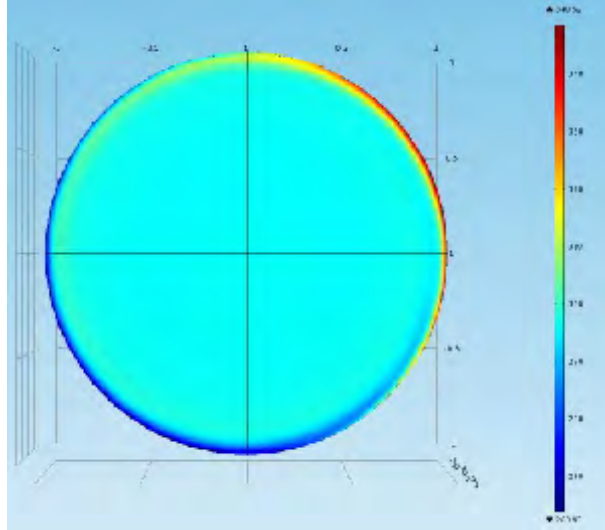


**FIG. 5** Equatorial cross section of temperature distribution. Rotation is CCW with solar illumination along the x-axis from the right. The warmest region is red and the coolest is blue.

of rotation increases (slower rotating body). This larger temperature variance across the body directly affects the magnitude of the radiative force; it will be shown later in the paper that the slower rotating spheres experience larger force values.

The temperature distribution of an equatorial slice of the model is shown in Figure 5. Illumination is from the right. The sphere is rotating counterclockwise so the change in temperature is visible from the warm red region, early “afternoon”, to the cool blue region just before “dawn”. The temperature propagation into the sphere is shallow with a penetration depth roughly constant for variously sized spheres. The skin depth near the surface is approximately a couple of centimeters near the surface, but the temperature continues to cool more slowly roughly over a one-meter distance. This effect varies somewhat with the period of rotation. A quantitative display of the penetration of the heat below the surface is given in Figure 6. The color coding is the same as in Figure 4. The slower rotations have the highest subsolar temperature and the lowest interior temperatures. Given this mostly diameter independent penetration depth for different sized spheres, we were able to “hollow” out the sphere for larger radii to allow for finer meshing schemes on the remaining shell. This was helpful in reducing computation times given our limitations on computational resources. We found a shell thickness between one and five meters to suffice for our computations.

The penetration has been studied for various sized spheres, of constant rotational period,

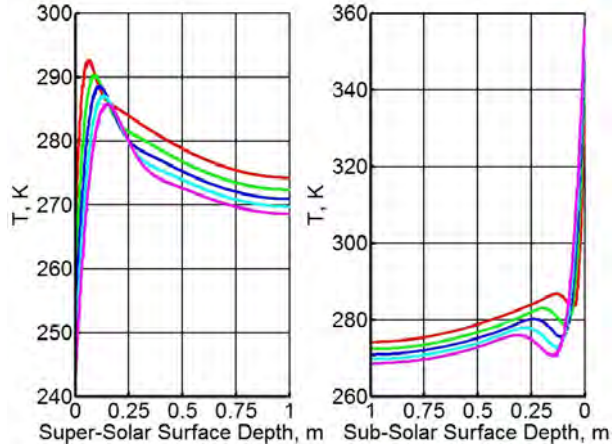


**FIG. 6** Penetration depth of heat for the subsolar region (right) and the supersolar region (left).

ranging from 2 m to 560 m in diameter. For the larger spheres there is a clearly defined layer where the temperature is the coolest at about 40 to 50 cm deep. The small spheres tend to stay near the low temperature while the interior of the larger spheres warms back up after a dip. There is about a 40 K drop between the surface temperature and the interior temperature for the larger spheres. In the night-time plot in Figure 6 (left) we see about a 17 K drop between the interior and the surface temperature. There is a smaller spread of temperature in the surface-to-interior difference at night than in daytime, as expected.

## 5. TEMPERATURE RESULTS

Figure 7 shows a typical plot of temperatures as dependent on the number of iterations where the time variable is referenced as the number of periods elapsed for  $90^\circ$  obliquity on the spherical model. Data are plotted for four different regions on the sphere. These data were taken from a simulation involving a two-meter diameter sphere, rotating with a period of 15,440s ( $\approx 4.3$  hrs, the rotation period of Bennu). Given a  $90^\circ$  in this run, the North Pole and South Pole have the same temperatures so only one of the values is reported here. There is transient behavior in the plotted temperature data when the distribution starts to develop. As time goes on, however, these dampen out and a stable distribution is reached, usually before 30 periods of rotation. The pole temperatures are still slightly decreasing after 30 periods of calculation and will do so for some time, but given that this simulation has a  $90^\circ$  obliquity, the contributions of these area's temperatures to the resultant force are canceled out by symmetry of the sphere about the equator

and orbit plane.

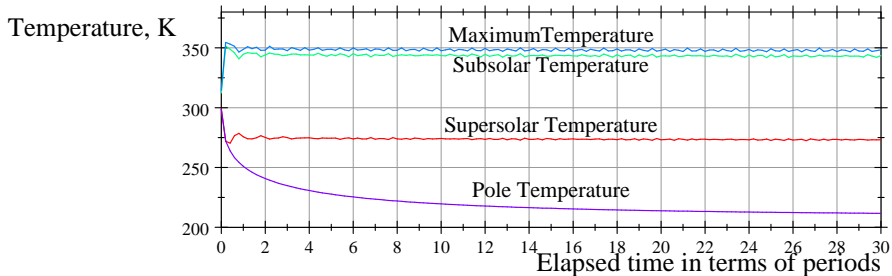


**FIG. 7** Temperature dependence upon the number of iterations.

### 5.1. Initial Temperature Analysis

After experimenting with the initial temperature value and its impact on the final temperature distribution, it was found that this parameter only affected the computation time to get consistent results. Figure 8 shows the maximum temperature values for several initial temperatures. After some length of time, the temperature distribution of the sphere becomes independent of the initial temperature assumed. Our numerous test plots extending for 30 periods of rotation show the length of time required to reach the final temperature distribution. Depending upon the period of rotation and initial temperature chosen for the body, 30 periods may or may not be enough time. Figure 8 shows how the maximum temperature behaves on a 2-m diameter sphere. The sphere was rotating with a period of 15440 s and positioned with  $90^\circ$  obliquity. For all five temperature curves plotted, they asymptotically approach the same temperature, suggesting that the specified initial temperature only influences how long it takes to achieve the desired equilibrium distribution necessary for an accurate force calculation (see Equation (20)). This behavior is also representative of the temperature behavior at the subsolar, supersolar, and pole locations on the sphere. Through more rigorous analyses we found 303 K to be the initial temperature to use on a sphere with Bennu thermal parameters.

### 5.2. Equatorial Temperature Observations

As we experimented with various radii, we found that temperature has little dependence upon diameter with all else being equal. Temperature does vary more strongly, however, with rotation period. In Figure 9 we show several curves for temperature over the equatorial region

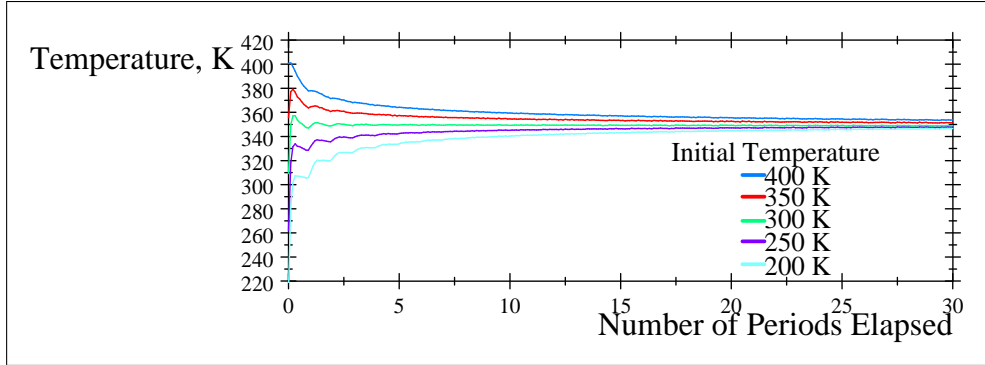


**FIG. 8** Convergence of maximum temperature of the hot spot for various initial values.

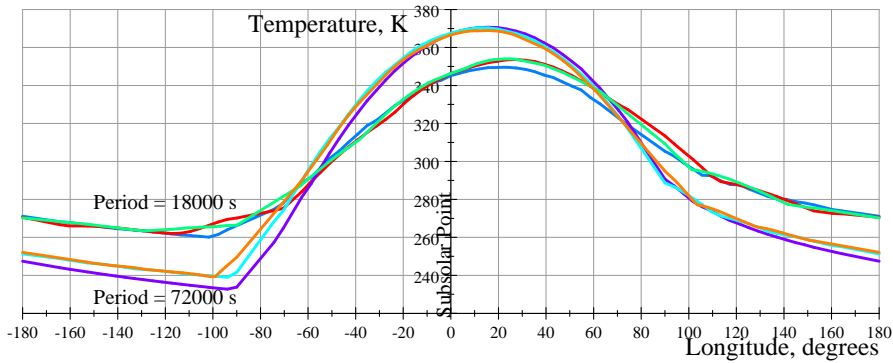


**FIG. 9** Temperature for two periods and three radii for each period.

for combinations of three radii and two rotation periods (in seconds). Overall the curves exhibit a cooling to the right of the “hot” region and continued cooling until early morning. Then when the sun starts shining on the material coming into the dawn side, the temperature starts to climb rather abruptly for the slower rotation.

There are three blended curves at the highest peak in the graph demonstrating that for a 72,000 s rotation period the subsolar equatorial temperature is independent of sphere diameter. On the dawn side we see slight variations for the three different radii for this period. The other three curves are for the faster rotation period of 18,000 seconds. These peaks are shifted to the right relative to the slower rotation indicating for faster rotations the hot spot moves farther away from the subsolar point as expected. Near the peaks of these three curves we see more radii dependence than for the slower rotation, but this dependence dissolves as the body cools. Just before dawn they again separate slightly over a short distance. The faster rotating bodies do not heat as much as the slower rotating bodies, but they do not cool as much either. For all six

curves, the physical parameters are the same except for the two parameters shown.

## 6. FORCE THEORY

Once we have the surface temperature distribution over the entire body we can calculate the force. A rigorous detailed way to do this is to use the Maxwell Stress Tensor [19, p. 239]. However, by not being concerned with the behavior of electric and magnetic fields over the body we can use the more macroscopic approach of radiative transfer [20, Chap. 3] using power as the basic quantity instead of electromagnetic fields. Our basic quantity is *specific intensity*,  $I_f(s, \Omega)$  represented by  $I_f$ , of radiated power in watts per meter squared per Hertz per solid angle,  $\Omega$ . Surface area is represented by  $s$ . The energy, in joules, radiated from a surface  $ds$  in the  $\theta$  direction (referenced to the surface normal) into a differential solid angle  $d\Omega$  is

$$dE_f = I_f \cos \theta ds df d\Omega dt. \tag{11}$$

where  $f$  is the frequency. We next apply the quantum mechanical expression for energy

$$E^2 = p^2 c^2 + m^2 c^4 \tag{12}$$

where  $p$  is the momentum of a particle,  $c$  is the velocity of light in a vacuum, and  $m$  is the mass of the particle. An important property of this equation is that it applies to continuous quantities as well as to point particles. In the case of radiation we are dealing with a photon whose mass is zero. We therefore get an expression for momentum as

$$dp = dE_f/c = I_f \cos \theta ds df d\Omega dt/c. \tag{13}$$

Now we can formulate pressure,  $P_r$ , using the definition that pressure caused by radiation is the net rate of transfer of momentum normal to, and across,  $ds$ . Thus

$$dP_r(f) = \frac{dp}{ds dt} \cos \theta. \tag{14}$$

This is the pressure due to radiation from a differential surface element. This element radiates isotropically into a hemisphere above it. We get the total outward pressure per unit frequency

at a point by integrating over the hemisphere above it:

$$P_r(f) = \frac{1}{c} \int I_f \cos^2 \theta d\Omega = \frac{1}{c} \int_0^{2\pi} \int_0^{\pi/2} I_f \cos^2 \theta \sin \theta d\theta d\phi. \quad (15)$$

Since we do not know the distribution of specific intensity over the hemisphere surrounding the point, we assume it is a constant with respect to angle, but it can vary with surface position. The pressure integral becomes

$$P_r(f) = \frac{I_f}{c} \int_0^{2\pi} \int_0^{\pi/2} \cos^2 \theta \sin \theta d\theta d\phi = \frac{I_f}{c} \frac{2\pi}{3}. \quad (16)$$

To get an expression for spectral intensity,  $I_f$ , we assume black body radiation which is given by

$$\pi I_f = \frac{2hf^3}{c^2} \frac{1}{e^{hf/kt} - 1} \quad (17)$$

where  $h$  is Plank's constant. The  $\pi$  to the left of  $I_f$  converts  $I_f$  from W/(m<sup>2</sup>Hz ster) to W/(m<sup>2</sup>Hz) to agree with the units of the Planck law. To find the intensity over all frequencies we integrate Planck's law and represent the result by  $I$  (no subscript). We have

$$\pi I = \int_0^{\infty} \frac{2hf^3}{c^2} \frac{1}{e^{hf/kt} - 1} df = \sigma T^4 \quad (18)$$

with units of W/m<sup>2</sup>. The last part of this expression is the Stefan-Boltzmann law where  $\sigma$  is the Stefan-Boltzmann constant. With this result we get the total pressure in the radial direction over all frequencies as

$$P_r = \int P_r(f) dv = \frac{2}{3c} \epsilon \sigma T^4 \quad (19)$$

in N/m<sup>2</sup>, where we have inserted the emission coefficient,  $\epsilon$ , since an asteroid is not a perfect black body radiator.

Finally we arrive at the force calculation. Given the results of the radial pressure over a differential surface of the body we discretely sum up individual contributions. The individual numbers come from a COMSOL numerical solution for temperature. COMSOL also gives the numerical value of each node in the mesh. These points are used to find the area of each small surface area segment  $A_i$  in the mesh. We use COMSOL to find the temperature distribution

and use our own software to convert the temperature to force. For each mesh segment in the temperature solution there is a temperature that is assigned a vector direction normal to the surface of the segment,  $\mathbf{n}_i$ . See Figure 2 for an illustration of vectors emanating normally to the mesh segments. The temperature vectors are converted to pressure using Equation (19) and summed with the formula

$$\mathbf{F} = \sum_{i=1}^N P_{r_i} \mathbf{n}_i A_i = \sum_{i=1}^N \frac{2}{3c} \epsilon_i \sigma T_i^4 \mathbf{n}_i A_i. \quad (20)$$

This is the equation we used in our own software once we solved for the surface temperature distribution with the COMSOL software. Spatial force components were calculated for each segment, then components were summed vectorily with the final  $F_x$ ,  $F_y$ , and  $F_z$  components used to calculate the total force magnitude and direction.

## 7. FORCE ANALYSIS

We discuss force dependence upon five things in the numerical analysis: 1) Step size, 2) mesh size, 3) obliquity of the incident solar angle, 4) period of sphere rotation, and 5) diameter of the sphere. All other parameters are the same as for Bennu. Due to the slight fluctuations in temperature even after a large number of iterations, we obtain stable reportable numerical results by averaging the results for the last five rotation periods.

Many computer simulations were made in determining which of the parameters specified in the asteroid model contribute to the Yarkovsky Effect. We have found the resultant force vector and its components to be related to the size of the sphere, the period of rotation, and the obliquity of the spin vector. The relationships between force and material properties are not considered here; we left the values of thermal conductivity  $k$ , density  $\rho$ , and heat capacity,  $C$ , to match the ones representative of Bennu, as described in the previous section. There are additional parameters required as inputs for the COMSOL simulation to run properly, but their only effects are on the length of simulation time required for achieving stable results, including initial temperature ( $T_0$ ), step size, number of steps, and meshing scheme.

TABLE 2

The composite force for runs with various numbers of mesh elements.

<b>Total No. of Elements</b>	<b>No. of Surface Elements</b>	<b>Force, <math>\mu\text{N}</math></b>
64	48	1.12
401	152	1.26
1136	240	1.53
2771	464	1.77
8516	848	1.98
16,726	1280	2.06
53,296	2776	2.04
208,835	6552	2.00
1,135,550	19664	2.05

### 7.1. Step Size Analysis

COMSOL gives us a choice of step size in the iterations. To test the effect of step size on the temperature results we made runs with six different step sizes. They were 30, 12, 10, 5, 2, and 1 step(s) per period. Once the number of steps per period is greater than five, there is no significant change in the final force calculation. Consequently, in subsequent runs we conservatively used 10 steps per period of rotation.

### 7.2. Mesh Size Analysis

Table 2 shows the resultant force magnitude corresponding to different tetrahedral mesh settings, all on a 2-m diameter sphere. We only report the number of total elements and surface elements here, as the names the COMSOL software has designated for the mesh settings (i.e. “Coarse”, “Normal”, or “Fine” meshing) are somewhat misleading. The sphere was rotating with a period of 15440 s, and a  $90^\circ$  obliquity. As the table shows, the resultant force magnitude is dependent upon the number (and also the size) of the elements. For most of the data presented in this paper 53,296 elements were used. However, in some cases 1,135,550 elements were needed. This table is only for tetrahedral meshing, but we did need to use a swept-meshing type for some of the calculations. Our swept meshing consisting of triangular facets layered between two surfaces was used on the large diameter simulations when a hollow sphere was required to conserve computational resources.

### 7.3. Force Equation Development

The radiative force acting on the asteroid is dependent upon several parameters including its material properties (Table 1) as well as its macroscopic properties. The period of rotation, relative inclination of the spin axis, orbital distance, and size of the body are analyzed in this section to show how they affect the resultant force. For the size of the body, we use the diameter of the sphere as the characteristic dimension,  $d$ . Beyond these idealizations the force results become unique to the orbiting bodies in question. The fitted force equations presented in this paper are meant to apply to any orbiting body that can be idealized or estimated as a sphere. After calculating the forces with Equation (20) using the COMSOL temperatures, we fit the forces to the equation

$$F'_{x,c} = A(\cos i)p^{c_1} |\mathbf{r}|^{c_2} \epsilon^{c_3} \alpha_{TP}^{c_4} \quad (21)$$

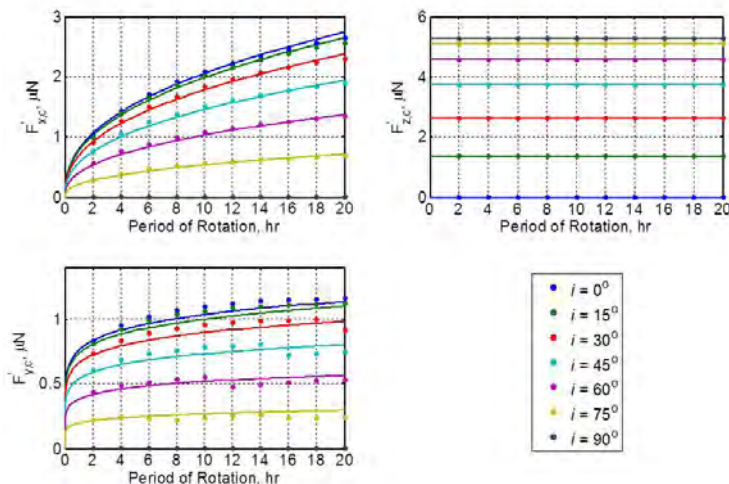
where each force factor is dependent upon a trigonometric transform of the obliquity and follows power regressions quite well for the other parameters; period of rotation, orbital distance, surface emissivity, and thermal parameter,  $\alpha_{TP}$ . This thermal parameter comes from simplifying the coefficients in the heat transfer Equation (1) when  $\rho$ ,  $C$ , and  $k$  are brought to one side so that  $\alpha_{TP} = \rho C/k$ . The period of rotation,  $p$ , is in seconds, the orbital distance,  $\mathbf{r}$  in astronomical units, the thermal parameter in  $\text{kg s/m}^2$ , the sphere diameter in meters, and the force values in Newtons. The coefficients and power values of the force component equations are found from linear regression fitting of

$$\ln \left( \frac{F'_{x,c}}{\cos i} \right) = \ln A + c_1 \ln p + c_2 \ln r + c_3 \ln \epsilon + c_4 \ln \alpha_{TP} \quad (22)$$

for each force component. After fitting the above equation to multiple COMSOL runs, the results, in matrix form, are

$$\begin{bmatrix} F_x \\ F_y \\ F_z \end{bmatrix}'_c = \begin{bmatrix} 4.82 \times 10^{-6} \cos i p^{0.415} |\mathbf{r}|^{-3.17} \epsilon^{1.81} \alpha_{TP}^{-0.330} \\ 1.04 \times 10^{-6} \cos i p^{0.135} |\mathbf{r}|^{-2.67} \epsilon^{1.35} \alpha_{TP}^{-0.0842} \\ 5.94 \times 10 \sin i |\mathbf{r}|^{-2.15} \epsilon^{1.12} \end{bmatrix} \left[ \left( \frac{d}{2} \right)^2 \right]. \quad (23)$$

This equation is for an asteroid with prograde rotation. If the asteroid is experiencing retrograde motion, the sign of  $F'_{y,c}$  is switched.



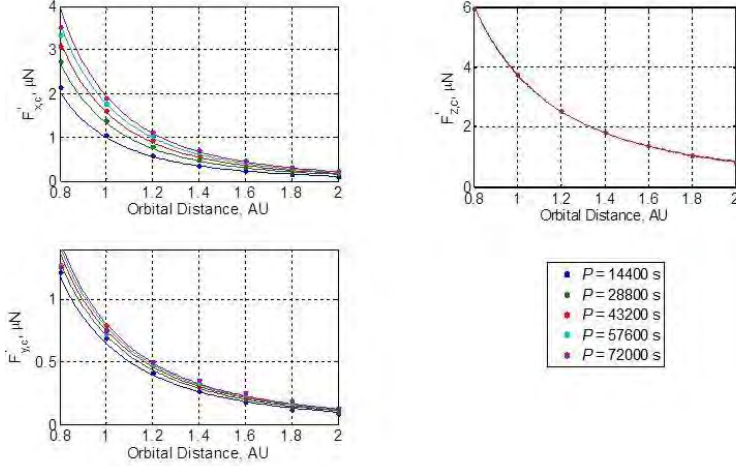
**FIG. 10** Force component plots for various periods of rotation and inclination (90 degrees minus obliquity) at orbital distance of 1 AU on a 2-m diameter sphere.

Figure 10 shows the calculated force component values (dots) as well as the fitted equations (smooth lines) from Equation (23) for various periods of rotation and inclinations on a 2-m diameter sphere, one AU from the sun. The period of rotation ranges from 2 to 20 hours in 2 hour increments with the inclination of the spin axis ranging from 0 to 90 degrees in 15 degree increments. The forces in the figures are in micro-Newtons. The  $x$ - and  $y$ -components of force increase with period of rotation but the  $z$ -component is not affected.

Figure 11 shows the force dependence upon orbital distance for a spherical asteroid 2 m in diameter. The sphere is at an obliquity of 45 degrees for the data shown with the force components plotted for various periods of rotation.

So far, the Yarkovsky force equations presented have been for a spherically idealized asteroid, 2 m in diameter. Including the diameter into these equations takes a lot of computing power in accurately analyzing the full range of practical sphere sizes (up to 500 m diameter for Bennu) and so, with this in mind, we present an alternate route that gives the same results in a quicker time frame. Starting with the original force equation (Equation (20)) and letting each cell have the same surface emissivity, as has been done with the model in COMSOL, the equation simplifies to

$$\mathbf{F} = \frac{2\epsilon\sigma}{3c} \sum_{i=1}^N T_i^4 \mathbf{n}_i A_i. \quad (24)$$



**FIG. 11** Force component plots for various periods of rotation and orbital distances on a 2-m diameter sphere at an inclination of 45 degrees.

Assuming that as the body increases in size, the temperature distribution on the surface does not change greatly, the force is only dependent on the surface area:

$$F \propto \sum_{i=1}^N A_i \propto d^2. \quad (25)$$

Figure 12 shows the force component dependence on the thermal parameter for a 2-m diameter sphere having a period of rotation of 36,000 s and orbiting at 1 AU. The  $x$ - and  $y$ -components show power regression trends while the  $z$  component shows no sign of dependence. Equation (23) shows the force dependence on the thermal parameter  $\alpha_{TP}$ .

The last variable to include in the resultant force equation is the surface emissivity where we continue to idealize the asteroid as behaving like a gray body. Figure 13 shows the force components over an emissivity sweep of a sphere with a 2-m diameter, 1 AU from the sun, and rotating with a period of 72,000 s. Equation (23) shows the force dependence on emissivity  $\varepsilon$ .

The force equation has been derived from specific cases in COMSOL. To make these component equations useful, they must be converted into the perifocal coordinate system; a coordinate system that defines the orbit plane. To obtain the force at a specific point in the orbit requires the true anomaly angle,  $\nu$ , the angle between the orbit plane and the COMSOL  $y$ -axis,  $\theta$ , and the inclination angle (compliment of obliquity). The Yarkovksy effect at an arbitrary position of a

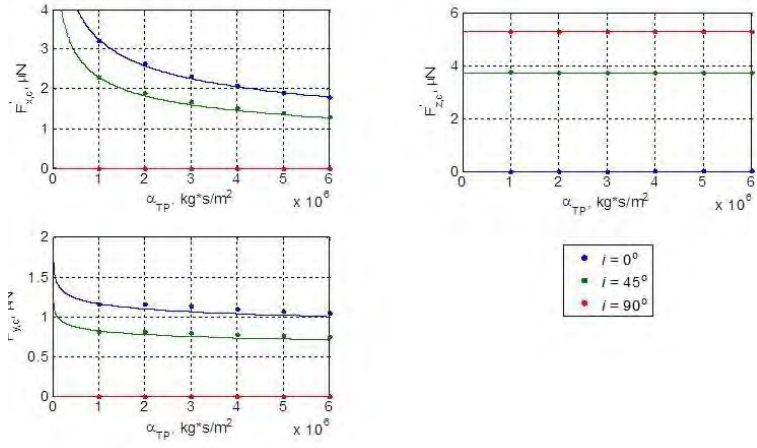


**FIG. 12** Force components vs thermal parameter for 36,000 s period of rotation and 2-m diameter sphere at 1 AU.

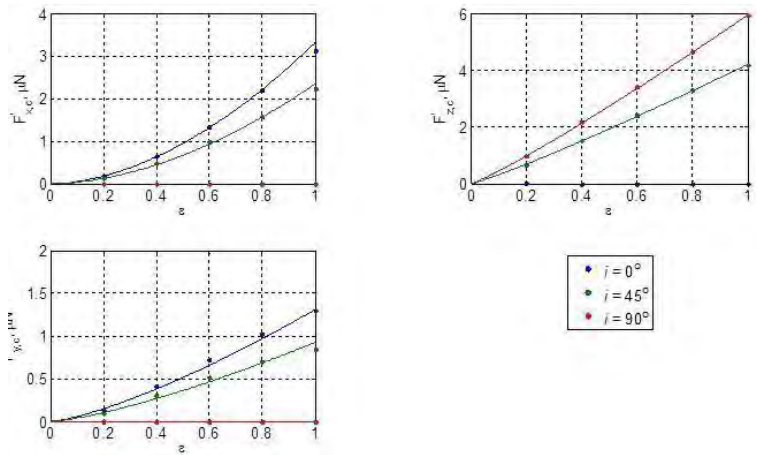


**FIG. 13** Emissivity results for a 2-m diameter sphere at 1 AU, rotating with a period of 72000 s.

spherically idealized asteroid's orbit is

$$\begin{bmatrix} F_p \\ F_q \\ F_w \end{bmatrix} = \begin{bmatrix} \cos \nu & -\sin \nu & 0 \\ \sin \nu & \cos \nu & 0 \\ 0 & 0 & 1 \end{bmatrix} \begin{bmatrix} 1 & 0 & 0 \\ 0 & \cos \theta & -\sin \theta \\ 0 & \sin \theta & \cos \theta \end{bmatrix} \begin{bmatrix} \cos \iota & 0 & \sin \iota \\ 0 & 1 & 0 \\ -\sin \iota & 0 & \cos \iota \end{bmatrix} \begin{bmatrix} F_x \\ F_y \\ F_z \end{bmatrix}'_c \quad (26)$$

where  $\nu$  is the anomaly angle and  $\theta$  is the angle between the orbit plane and the COMSOL y-axis.

The angles are calculated using

$$\nu = \cos^{-1} \left( \frac{\mathbf{e} \cdot \mathbf{r}}{|\mathbf{e}| |\mathbf{r}|} \right) \quad (27)$$

$$\theta = \cos^{-1} \left( \frac{\mathbf{h} \cdot \mathbf{y}_{comsol}}{|\mathbf{h}|} \right) \quad (28)$$

$$\mathbf{y}_{comsol} = \frac{\mathbf{s} \times \mathbf{r}}{|\mathbf{s} \times \mathbf{r}|} \quad (29)$$

where  $\mathbf{e}$  is the eccentricity vector,  $\mathbf{r}$  is the radial position vector,  $\mathbf{h}$  is the angular momentum vector, and  $\mathbf{s}$  is the spin vector. The spin vector of the asteroid is converted to the same coordinate system by a transformation using the longitude angle,  $\lambda$ , and latitude angle,  $\beta$ , measured from the orbit plane normal direction:

$$\mathbf{s} = \begin{bmatrix} \cos \lambda & -\sin \lambda & 0 \\ \sin \lambda & \cos \lambda & 0 \\ 0 & 0 & 1 \end{bmatrix} \begin{bmatrix} \cos \beta & 0 & \sin \beta \\ 0 & 1 & 0 \\ -\sin \beta & 0 & \cos \beta \end{bmatrix} \begin{bmatrix} 0 \\ 0 \\ 1 \end{bmatrix}. \quad (30)$$

With the force equation now fully defined in an orbital framework, the orbital effects can be determined.

## 8. ORBITAL PERTURBATIONS

The three force components in the orbital reference frame oscillate over an orbit because the asteroid's path is elliptical. The orientation of the spin axis determines the general trends of the components. If the spin axis is oriented to be coincident with the P direction, the "seasonal effect", the three force trends closely resemble sine and cosine waves. If the spin axis is oriented to be coincident with the W direction, the "diurnal effect", the  $F_w$  component is equal to zero and the  $F_p$  and  $F_q$  components resemble phased sine and cosine waves. However, in both of these

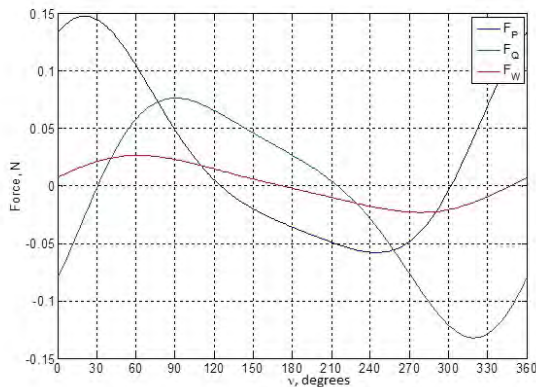


**FIG. 14** History of Yarkovsky force on Bennu.

TABLE 3  
Orbit Properties of Bennu

Parameter	Value
$a$	1.1260 AU
$e$	0.2037
mass	$7.8 \times 10^{10}$ kg
$\beta$	$-6.02^\circ$
$\lambda$	$92.17^\circ$

examples, note that while the trends resemble the trigonometric functions, the peak and trough values will not necessarily be equal in magnitude due to the force dependence on orbit distance as well. Only in a circular orbit will the trends be identical to phased sine and cosine waves.

Looking closely now at the orbit of Bennu, we note that the orbit is elliptical and the spin axis is not in a unit vector direction. This orbit is more complex and so too are the force trends, as can be seen in Figure 14. The orbital parameters used are shown in Table 3 with the spin axis angles taken from Müller et al. [13]. The material properties used for this were shown previously in Table 1 and the final parameters required, diameter and period of rotation, are 510 m and 4.298 hr, respectively. However, when calculating force using Equations (23) and (26) we used the new density  $1260 \text{ kg/m}^3$  as given by Chesley et al. [16] rather than  $2000 \text{ kg/m}^3$  as used in the derivation of Equation (23).

We can see how, even with a small latitude angle of  $-6.02^\circ$ , the W-component is already pronounced. The P and Q components have also deviated from a simple sine or cosine wave. The P component reaches its maximum value at approximately the  $20^\circ$  and a minimum around

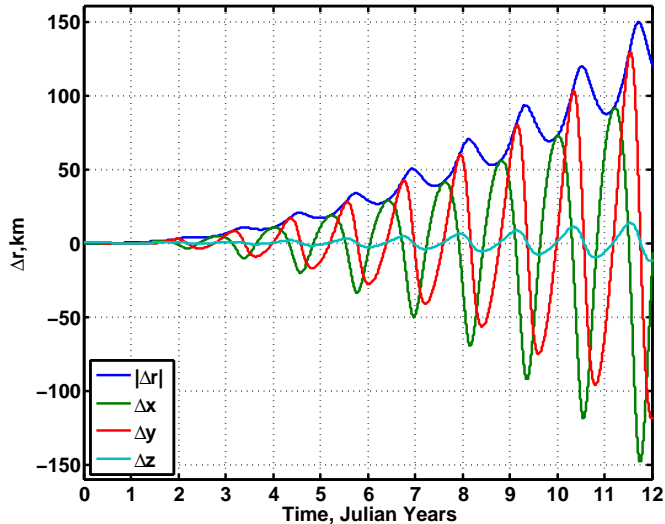


**FIG. 15** Change in expected position of Bennu due to the Yarkovsky effect over a 12-year period.

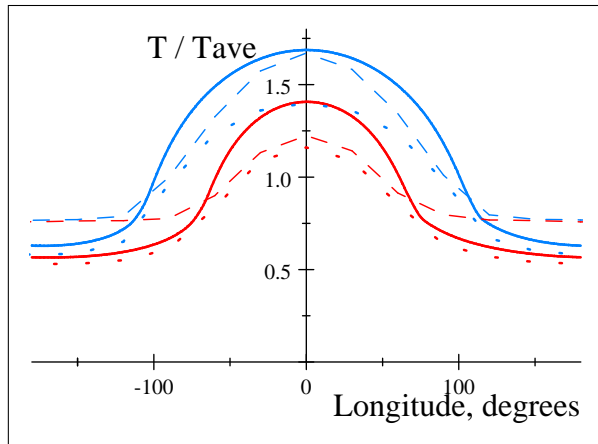
the  $240^\circ$  true anomaly angle. As is also evident by the quick rise and drop between the peak and trough, the phase is skewed. However, this pattern is not out of the ordinary because of the elliptical orbital path and the focal reference point the anomaly angle is measured from. The  $F_q$  component behaves almost completely opposite to the  $F_p$  component. They do exhibit very similar trends except that they are reversed and have slightly different magnitudes.

Figure 14 shows the force data for a single orbit, during which the orbit hardly changes. The change in orbit is more evident for longer time periods. Extending the simulation to a 12 Julian year cycle, Figure 15 shows the change in expected orbit position due to the Yarkovsky Effect. These results have been calculated for a 2-body gravitation problem using a non-stiff ordinary differential equation solver in MATLAB, ODE113. The maximum displacement at the end of the run is 150 km from the otherwise expected position.

We observed earlier that temperature is weakly dependent upon diameter, hence, according to Equation (20) the force will vary only with surface area. Since area goes as  $r^2$ , we expect the force to go as  $r^2$  which we have seen from our calculations of force from the COMSOL temperatures.

## 9. TEMPERATURE COMPARISON WITH PREVIOUSLY PUBLISHED FORCES

Sekiya et al. [7] compared their iterative results for temperature vs. longitude with results from Vokrouhlický [17] in plots in their Figs. 4 and 5. We extracted numerical values from their plots, combined our results with them, and show the results in Figs. 16 and 17. Our calculations for these figures use Bennu parameters except we used a two-meter diameter sphere, and a period of 24,704 seconds in Figure 16 and a period of 24,040 seconds in Figure 17. Sekiya et al. [7] use global parameters in their results so our periods were chosen to put our results on the same scale as theirs. Looking at Figure 16 we see that our result at  $\phi = 0^\circ$  and  $\theta = 60^\circ$  is similar to that of Vokrouhlický. However, away from center, our results are warmer, but again resemble Vokrouhlický's on the nightside. On the other hand at  $\phi = 0^\circ$  and  $\theta = 120^\circ$  our results are definitely warmer than those of Sekiya, et al. and of Vokrouhlický, but drop off more sharply near the limb. On the nightside for  $120^\circ$  our results are similar to those of Sekiya, et al. and Vokrouhlický's results are clearly warmer than the other two results. Figure 17 shows a delay in heating, but otherwise the relative relationships between the three sets of results remain the same as in Figure 16. Our temperature results are always greater than or equal to, the results of the other authors in the sunlit region.



**FIG. 16** Plot of temperature distribution for latitudes 60 degrees (blue) and 120 degrees (red). Solid line is from COMSOL results, dotted line from Sekiya et al, and dashed line from Vokrouhlický.

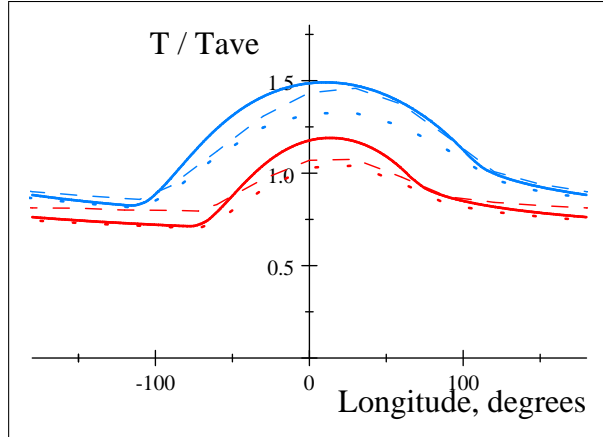


**FIG. 17** Same as Fig. 17, but with a thermal lag.

TABLE 4  
Comparison of Bennu and Golevka

Parameter	6489 Golevka	Bennu
Semi-major axis, AU	2.4995 [24]	1.2160
Dimension, m	530 [22]	510
Mean density, kg/m <sup>3</sup>	2700 [21]	1260
Mass, $\times 10^{10}$ kg	21 [21]	$7.8 \pm 0.9$
Rotation period, hr	6.026 [23]	4.289
Albedo	0.151 [22]	0.01
Thermal conductivity, W/(m K)	0.01 [21]	0.3
Temperature, K	$\sim 176$	$\sim 350$

## 10. COMPARISON OF BENNU WITH 6489 GOLEVKA

Since 6489 Golevka is an asteroid of similar size to Bennu and has known parameters, it is of interest to compare its parameters with those of Bennu. We do this in Table 4. Although the dimension is about the same, other parameters vary considerably, especially the density and the distance from the sun. However, the distance from the sun does not come close to accounting for the difference in temperature. If we scale the 350 K of Bennu to the square of the ratio of semi-major axes of the orbits, Golevka’s temperature would be 83 K. With a higher albedo of about a factor of 15, Golevka would be even significantly cooler than 83 K. We are left with density and thermal conductivity as the major reasons for the warmer surface of Golevka. There is less heat conducted into the body, and more surface mass to absorb solar radiation.

## 11. CONCLUSIONS

The numerical solutions given by the COMSOL Multiphysics software are in reasonably agreement with previously published results and are quite possibly more correct than the analytic results since there are no theoretically built in approximations. We showed how the Yarkovsky effect is related to the size, period of rotation, and obliquity of a sphere having thermal conductivity of  $0.3 \text{ W}/(\text{m K})$ , density of  $2,000 \text{ kg}/\text{m}^3$ , and heat capacity of  $600 \text{ J}/\text{K}$  at a distance of 1 AU from the sun. Approximating the asteroid Bennu as a sphere of homogenous composition, the magnitude of the Yarkovsky force at perihelion is  $0.083 \text{ N}$  at an orbital distance of  $0.897 \text{ AU}$ . The maximum displacement of the asteroid over 12 years due to the Yarkovsky effect is  $150 \text{ km}$ . With the flexibility of COMSOL, in the future it will be possible to evolve the spherical homogeneous model into more realistic versions of an asteroid. The seasonal effect due to orbital motion can be included as well. The work reported here is in a preliminary stage. We are continuing with extensive modeling with elongated objects and rough surfaces. These results will contribute towards improving predictions of orbital changes of near-Earth objects (NEOs). One of the objectives of NASA's OSIRIS-Rex mission (to be launched in 2016, to reach the asteroid in 2020, and return samples to Earth in 2023) is to directly measure its Yarkovsky acceleration. With improved measurements of the physical properties of Bennu and refinement of analytical and numerical techniques, accuracy of predicted forces will steadily improve for many (NEOs).

## 12. ACKNOWLEDGMENTS

We thank Ikenna C. Niebedim for significant assistance with setting up COMSOL jobs. We also thank Mian Qin from COMSOL for helping us with the swept mesh analysis, and William Meeker for help in understanding multiple regression. We thank the Department of Electrical and Computer Engineering at Iowa State University for supporting the COMSOL multiphysics package and the heat transfer package.

## REFERENCES

- [1] Milani, A., Chesley, R. C., Sansaturui, M. E., Bernardi, F., Valsecchi, G. B., and Arratia, O., "Long Term Impact Risk for (101955) 1999 RQ<sub>36</sub>," *Icarus*, Vol. 203, 2009, pp. 460-471.

- [2] Basart, J., Goetzke, E., Setzer, C., Wie, B., “Modeling and Estimating the Yarkovsky Effect on Asteroid 1999RQ36”, AIAA 2012-5058, AIAA Guidance, Navigation, and Control Conference, August 2012.
- [3] Farinella, P., Vokrouhlický, D., and Hartmann, W. K., “Meteorite Delivery via Yarkovsky Orbital Drift,” *Icarus*, Vol. 132, 1998, pp. 378-387.
- [4] Vokrouhlický, D., “A Complete Linear Model for the Yarkovsky Thermal Force on Spherical Asteroid Fragments,” *Astron. Astrophys.*, Vol. 344, 1999, pp. 362-366.
- [5] Bottke, Jr., W. F., Rubincam, D. P., and Burns, J. A., “Dynamical Evolution of Main Belt Meteoroids: Numerical Simulations Incorporating Planetary Perturbations and Yarkovsky Thermal Forces,” *Icarus*, Vol. 145, 2000, pp. 301-331.
- [6] Žižka, J., and Vokrouhlický, D., “Solar Radiation Pressure on (99942) Apophis,” *Icarus*, Vol. 211, 2011, pp. 511=518.
- [7] Sekiya, M., Shimoda, A. A., and Wakita, S., “An Iterative Method for Obtaining a Nonlinear Solution for the Temperature Distribution of a Spinning Spherical Body Irradiated by a Central Star,” *Plan. Space Sci.*, Vol. 60, 2012, pp. 304-313.
- [8] Rozitis, B. and Green, S. F., “Directional Characteristics of Thermal–Infrared Beaming from Atmosphereless Planetary Surfaces—a New Thermophysical Model,” *Mon. Not. R. Astron. Soc.*, Vol. 415, 2011, pp. 2042-2062.
- [9] Rozitis, B. and Green, S. F., “The Influence of Rough Surface Thermal–Infrared Beaming on the Yarkovsky and YORP Effects,” Vol. 423, 2012, pp. 367-388.
- [10] Čapek, D., Vokrouhlický, D., 2005. “Accurate model for the Yarkovsky effect.” In: Knežević, Z., Milani, A. (Eds.), *IAU Colloq. 197: Dynamics of Populations of Planetary Systems*, pp. 171–178.
- [11] <http://www.comsol.com/>.
- [12] Delbo, M., dell’Oro, A., Harris, A. W., Mottola, S., and Muller, M., “Thermal Inertia of Near-Earth Asteroids and Implications for the Magnitude of the Yarkovsky Effect,” *Icarus*, Vol. 190, 2007, pp. 236-249.

- [13] Müller, T. G., O'Rourke, L., Barucci, A. M., Pál, A., Zeidler, P., Altieri, B., González-García, and Küppers, M., "Physical Properties of OSIRIS-REx Target asteroid (101955) 1999 RQ<sub>36</sub> derived from Herschel, ESO-VISIR and Spitzer observations." *Astronomy and Astrophysics*, Vol. 548, 2012, pp. A36-A44.
- [14] Nolan, M. C., et al., "Shape Model and Surface Properties of the OSIRIS-REx Target Asteroid (101955) Bennu from Radar and Lightcurve Observations," *Icarus*, Vol. 236, 2013, pp. 629-640.
- [15] Emery, J. P., et al., "Thermal Infrared Observations and Thermophysical characterization of OSIRIS-REx Target Asteroid (101955) Bennu," *Icarus*, Vol. 234, 2014, pp. 17-35.
- [16] Chesley, S. R., et al., "Orbit and Bulk Density of the OSIRIS-REx Target Asteroid (101955) Bennu," *Icarus*, Vol. 235, 2014, pp. 5-22.
- [17] Vokrouhlický, D., "Diurnal Yarkovsky Effect as a Source of Mobility of Meter-sized Asteroidal Fragments: I. Linear Theory," *Astron. Astrophys.*, Vol. 335, 1998, pp. 1093-1100.
- [18] Delbo, M. and Michel, P., "Temperature History and Dynamical Evolution of (101955) 1999 Bennu: A Potential Target for Sample Return from a Primitive Asteroid," *Astroph. J. Lett.*, Vol. 728, 2011, pp. L42-L46.
- [19] Jackson, J. D., *Classical Electrodynamics*, 2nd ed., John Wiley & Sons, 1975.
- [20] Schott, J. R., *Remote Sensing: The Image Chain Approach*, Oxford Univ. Press, 1997.
- [21] Chesley, S. R., et al. "Direct Detection of the Yarkovsky Effect by Radar Ranging to Asteroid 6489 Golevka," *Science*, Vol. 302, 2003, pp. 1739-1742.
- [22] Hudson, et al., "Radar Observations and Physical Model of Asteroid 6489 Golevka," *Icarus*, Vol. 148, 2000. pp. 37-51.
- [23] Mottola, S. A., "Physical Model of Near-Earth Asteroid 6489 Golevka (1991 JX) from Optical and Infrared Observations," *Astron. J.*, Vol. 114, 1997, pp. 1234-1245.
- [24] D. Vokrouhlicky, A. Milani, S. R. Chesley, "Yarkovsky Effect on Small Near-Earth Asteroids: Mathematical Formulation and Examples," *Icarus*, Vol. 148, 2000, pp. 118-138.